Nonlinear Fourier Analysis of Free-Surface Buoy Data Using the Software Library FNFT

Wahls, S.; Brühl, M.; Fan, Yang-Ming; Huang, Ching-Jer

DOI
10.1115/OMAE2020-18676

Publication date
2020

Document Version
Accepted author manuscript

Published in
Proceedings of the ASME 39th International Conference on Ocean, Offshore and Arctic Engineering

Proceedings of the ASME 39th International Conference on Ocean, Offshore and Arctic Engineering OMAE 2020 June 28 – July 3, 2020, Fort Lauderdale, FL, USA

OMAE2020-18676

NONLINEAR FOURIER ANALYSIS OF FREE-SURFACE BUOY DATA USING THE SOFTWARE LIBRARY FNFT

Sander Wahls[1,*], **Markus Bruehl**[1], **Yang-Ming Fan**[2] **and Ching-Jer Huang**[2]
[1]Delft Center for Systems and Control, TU Delft, The Netherlands.
[2]Coastal Ocean Monitoring Center, National Cheng Kung University, Tainan, Taiwan.

ABSTRACT

Nonlinear Fourier Analysis (NFA) is a powerful tool for the analysis of hydrodynamic processes. The unique capabilities of NFA include, but are not limited to, the detection of hidden solitons and the detection of modulation instability, which are essential for the understanding of nonlinear phenomena such as rogue waves. However, even though NFA has been applied to many interesting problems, it remains a non-standard tool. Recently, an open source software library called FNFT has been released to the public. (FNFT is short for "Fast Nonlinear Fourier Transforms".) The library in particular contains code for the efficient numerical NFA of hydrodynamic processes that are approximately governed by the nonlinear Schroedinger equation with periodic boundary conditions. Waves in deep water are a prime example for such a process. In this paper, we use FNFT to perform an exemplary NFA of typhoon data collected by wave buoys at the coast of Taiwan. Our goals are a) to demonstrate the application of FNFT in a practical scenario, and b) to compare the results of a NFA to an analysis based on the conventional linear Fourier transform. The exposition is deliberately educational, hopefully enabling others to use FNFT for similar analyses of their own data.

INTRODUCTION

In 1967, Gardner et al. found an ingenious new method to solve the Korteweg-de Vries (KdV) equation [1]. Their approach was soon after extended to the nonlinear Schroedinger equation (NSE) by Zakharov and Shabat [2]. Today, many important nonlinear evolution equations are known to be solvable in this way, which is traditionally called inverse scattering transform method. However, since scattering transforms generalize the conventional Fourier transform, today often the term *nonlinear Fourier transforms (NFTs)* is used instead. NFTs offer interesting possibilities for data analysis that can reveal nonlinear effects hidden from conventional linear analysis. In the area of water wave data analysis, Osborne and coworkers have created a large body of pioneering work, much of which is contained in the book [3]. It is important to point out that there is not one NFT that covers all cases. On the contrary, the NFT is specific to the assumed nonlinear evolution equation (e.g., KdV or NSE) and boundary conditions. Furthermore, the mathematics behind NFTs is unfamiliar to many engineers. Despite many interesting results (see, e.g., [4,5,6,7,8,9,10,11,12,13]), NFT-based data analysis is thus not widely used at the moment.

The goal of this paper is to foster the general adoption of NFT-based analysis. We summarize many of the smaller details which are usually spread through the literature in one place. Furthermore, we explicitly show how the software library *FNFT* [14] can be used to perform an analysis of deep water data using the NFT for the periodic NSE. Our hope is that this exposition will enable engineers unfamilar with NFTs to perform their own analysis quickly.

The paper is structured as follows. In the next two sections, the theoretical background beyond the NSE and the NFT for the periodic NSE is provided. Then, the physical

*Address all correspondence to this author. Email: s.wahls@tudelft.nl.

interpretation of this NFT is discussed. Finally, we discuss the software library FNFT and demonstrate an analysis of free surface buoy data recorded before the coast of Taiwan using both the NFT and the linear Fourier transform.

THE NONLINEAR SCHROEDINGER EQUATION (NSE)

Wave trains

We consider the surface elevation of a unidirectional modulated wave train [15, Ch. 17.7],

$$a(x,t) = \mathrm{Re}\left[A(x,t)\,\mathrm{e}^{\mathrm{i}(k_0 x - \omega_0 t)}\right], \tag{1}$$

where x denotes location, t denotes time, $\mathrm{Re}[\cdot]$ denotes the real part and e and i denote Euler's and the imaginary number, respectively. We assume that the complex envelope $A(x,t)$ of the wave train is bandlimited, i.e., the two-dimensional Fourier transform $\hat{A}(k,\omega)$ of $A(x,t)$ satisfies

$$\hat{A}(k,\omega) := \int_{-\infty}^{\infty}\int_{-\infty}^{\infty} A(x,t)\,\mathrm{e}^{-\mathrm{i}(kx+\omega t)}\,\mathrm{d}k\,\mathrm{d}\omega = 0 \tag{2}$$

whenever $|k| > K$ or $|\omega| > \Omega$. Here, the constants $K, \Omega > 0$ denote the half-bandwidths w.r.t. to the location and time variables, respectively. We assume that $|k_0| \gg K$ and $|\omega_0| \gg \Omega$ such that $a(x,t)$ changes much faster than $A(x,t)$ in both time and space. Under these assumptions, the complex envelope $A(x,t)$ of a surface elevation can be recovered using the Hilbert transform [16, p. 491], [3, Ch. 13]

$$A(x,t)\,\mathrm{e}^{\mathrm{i}(k_0 x - \omega_0 t)} = a(x,t) - \mathrm{i}\,\mathscr{F}_t^{-1}\left[\mathrm{i}\,\mathrm{sign}(\omega)\mathscr{F}_t[a](\omega)\right](t), \tag{3}$$

where $\mathscr{F}_t[a](\omega) = \int_{-\infty}^{\infty} a(t)\,\mathrm{e}^{-\mathrm{i}\,\omega t}\,\mathrm{d}t$ and $\mathscr{F}_t^{-1}$ denote the Fourier transform w.r.t. t and its inverse, respectively, and $\mathrm{sign}(\omega) = 1$ for $\omega \geq 0$ and $\mathrm{sign}(\omega) = -1$ for $\omega < 0$.

Spatial NSE

Under the additional assumptions that the water is deep and the complex envelope is small, the complex envelope obeys the *spatial NSE* (see, e.g., [17, 18, 15, 3])

$$\mathrm{i}\left[A_t + C_g A_x\right] + \mu A_{xx} + \nu|A|^2 A = 0, \tag{4}$$

where the subscripts indicate partial derivatives. The values of the coefficients for gravity waves in water of infinite depth were derived by Zakharov [17], [3, Ch. 2.5.3]:

$$C_g = \frac{\omega_0}{2k_0}, \quad \mu = -\frac{\omega_0}{8k_0^2}, \quad \nu = -\frac{\omega_0 k_0^2}{2}. \tag{5}$$

Hasimoto and Ono derived coefficients for water of finite depth h [18], [3, Ch. 2.5.2]. With $\omega_0^2 = g k_0 \sigma$, $\sigma = \tanh(k_0 h)$ and g denoting gravitational acceleration, they are given by

$$C_g = \frac{c}{2}\left[1 + \frac{(1-\sigma^2)k_0 h}{\sigma}\right] \quad \text{where} \quad c := \frac{\omega_0}{k_0}, \tag{6}$$

$$\mu = \frac{-g}{8k_0\sigma\omega_0}\left\{\left[\sigma - k_0 h(1-\sigma^2)\right]^2 + 4k_0^2 h^2 \sigma^2 (1-\sigma^2)\right\}, \tag{7}$$

$$\nu = \frac{-k_0^4}{2\omega_0}\left(\frac{c}{2\omega_0}\right)^2 \left\{\frac{(9 - 10\sigma^2 + 9\sigma^4)}{2\sigma^2}\right. \tag{8}$$

$$\left. + \frac{4c^2 + 4(1-\sigma^2)cC_g + gh(1-\sigma^2)^2}{C_g^2 - gh}\right\}. \tag{9}$$

In what follows, we shall assume that $\mu\nu > 0$. With respect to the coefficients (6)–(8), that is $k_0 h \gtrapprox 1.363$ [18, p. 807].

This condition is necessary for the existence of both envelope solitons [15, Ch. 17.8] and modulational instabilities [15, Ch. 17.7], [13, Sec. 3.2]. (The case $\mu\nu < 0$ is obtained e.g. by multiscale-avering the KdV equation [19].)

Temporal NSE

The spatial NSE however is not suitable for our purposes (time series analysis). To arrive at a suitable temporal NSE, we follow [3, Ch. 12.2]. Since $A_t + C_g A_x \simeq 0$ at leading order (e.g., [20, Eq. 26], [21, p. 612]),

$$A_{xx} = (A_x)_x \simeq (-C_g^{-1} A_t)_x = -C_g^{-1}(A_x)_t \simeq C_g^{-2} A_{tt}. \tag{10}$$

We substitute this approximation in (4) and multiply both sides of the resulting equation with C_g^{-1}. This leads to the *temporal NSE*, which is suitable for time-series analysis:

$$\mathrm{i}\left[C_g^{-1} A_t + A_x\right] + \mu C_g^{-3} A_{tt} + \nu C_g^{-1}|A|^2 A = 0. \tag{11}$$

Note that since the roles of x and t are reversed in the temporal NSE, k_0 and ω_0 should be switched in (3) [3, 13.5].

Normalized Temporal NSE

We now bring the temporal NSE into a normalized form that typically used in the NFT-related literature. The following change of coordinates will be used [3, Ch. 12.2],

$$X = \frac{\mu}{C_g^3} x,\ T = t - \frac{x}{C_g},\ u(X,T) = \rho A(X,T),\ \rho := \sqrt{\frac{C_g^2 \nu}{2\mu}}. \tag{12}$$

First, we substitute $A = \rho^{-1} u$ in the temporal NSE (11):

$$\mathrm{i}\rho^{-1}\left[C_g^{-1} u_t + u_x\right] + \mu C_g^{-3}\rho^{-1} u_{tt} + \nu C_g^{-1}\rho^{-3}|u|^2 u = 0. \tag{13}$$

We multiply both sides of (13) with $\mu^{-1}C_g^3\rho$ and simplify the result using the relation

$$\frac{\mu}{C_g^3}\rho^{-1} = \frac{\mu}{C_g^4}\left(\frac{\nu}{2\mu}\right)^{-1/2} = \frac{\nu}{2C_g^4}\left(\frac{\nu}{2\mu}\right)^{-3/2} = \frac{\nu}{2C_g}\rho^{-3}. \quad (14)$$

This leads us to

$$\mathrm{i}\,\mu^{-1}C_g^3\left[C_g^{-1}u_t + u_x\right] + u_{tt} + 2|u|^2u = 0. \quad (15)$$

Applying the multi-dimensional chain rule to (12) shows that

$$u_t = u_X X_t + u_T T_t = 0 + u_T, \quad (16)$$
$$u_{tt} = (u_T)_t = u_{TX}X_t + u_{TT}T_t = 0 + u_{TT}, \quad (17)$$
$$u_x = u_X X_x + u_T T_x = \frac{\mu}{C_g^3}u_X - \frac{1}{C_g}u_t. \quad (18)$$

We substitute these relations in (15) and finally arrive at

$$\mathrm{i}\,u_X + u_{TT} + 2|u|^2u = 0. \quad (19)$$

This is the *normalized temporal NSE*.

THE NONLINEAR FOURIER TRANSFORM (NFT) FOR THE PERIODIC NSE

The first NFT for the NSE by Zakharov and Shabat [2] considered vanishing boundary conditions for the non-evolutionary variable. With respect to the normalized temporal NSE (19), that is $|u(X,T)| \to 0$ fast enough whenever $T \to \pm\infty$. For water waves, however often (but not always) periodic boundary conditions are more appropriate:

$$u(X, T+\ell) = u(X,T) \quad \text{for all } X, T, \quad (20)$$

where $\ell > 0$ is the period. In the following, we review the basics of the NFT for the periodic NSE [assuming $\mu\nu > 0$].

Finite gap solutions to the NSE

The theory of the NFT with periodic boundary condition (20) is centered around a special class of solutions known as *finite gap* (or band) *solutions* [22]. The most common form for the NSE (19) is due to Kotlyarov [23], where

$$[\log u(X,T)]_T = 2\mathrm{i}\sum_{k=1}^{n}\mu_k(X,T) + 2\mathrm{i}K,\ K = -\frac{1}{2}\sum_{k=1}^{2n+2}E_k. \quad (21)$$

Here, the E_k are certain complex constants that form the *main spectrum* and the μ_k are *auxiliary functions* that satisfy

$$[\mu_k]_T = -2\mathrm{i}\,\frac{\vartheta_k\sqrt{P(\mu_k)}}{\prod_{j\neq k}(\mu_k - \mu_j)}, \quad P(z) := \prod_{j=1}^{2n+2}(z - E_j), \quad (22)$$

$$[\mu_k]_X = 4\mathrm{i}\left(\sum_{j=1}^{n}\mu_j + K - \mu_k\right)\frac{\vartheta_k\sqrt{P(\mu_k)}}{\prod_{j\neq k}(\mu_k - \mu_j)}. \quad (23)$$

The *Riemann sheet indices* $\vartheta_k = \vartheta_k(X,T) \in \{\pm 1\}$ are signs that change when the corresponding $P(\mu_k)$ crosses the chosen branch cut of the square root function, which typically is the negative part of the real axis. (Technically, the μ_k evolve on a Riemann surface with two branches. The sheet index indicates the branch.) By integrating (21), we find that

$$u(X,T) = u(X,T_0)\exp\left(2\mathrm{i}\sum_{k=1}^{n}\int_{T_0}^{T}\mu_k(X,\tau)\,\mathrm{d}\,\tau - 2\mathrm{i}K(T - T_0)\right), \quad (24)$$

where T_0 is an arbitrary base point. A few remarks:

- The main spectrum $\{E_k\}_{k=1}^{2n+2}$ is independent of X and T. Only the auxiliary spectrum $\{\mu_k(X,T)\}_{k=1}^{n}$ changes.
- The points in the main spectrum form pairs, which are connected by curves in the complex plane known as *spines* (or bands).
- Two points in the main spectrum might be connected by a spine of length zero, so that they share the same position. In that case, the main spectrum point(s) are called *degenerate*. Degenerate points in the main spectrum may trap a point in the auxiliary spectrum that cannot move and thus does not contribute to the signal.

Fig. 1 shows the main spectrum, the loci of the auxiliary spectrum and the spines for the following perturbed plane wave initial condition (coefficients taken from [10])

$$u(X_0,T) = 1 + \varepsilon\,\mathrm{e}^{-0.822\,\mathrm{i}\,T}, \quad \ell = \frac{2\pi}{0.822}, \quad (25)$$

with parameters $\varepsilon = 0$ and $\varepsilon = 0.22$, respectively. In the unperturbed case shown in Fig. 1(left), we see two non-degenerate points in the main spectrum (blue circles) at $\pm\mathrm{i}$ that are connected by a spine (thick red line). On this spine are four degenerate main spectrum points. The complete auxiliary spectrum (black dots) is trapped by degenerate main spectrum points and thus does not contribute to the signal. Equation (21) hence implies that $[\log u]_T$ must be constant, which is indeed the case: $[\log u]_T = [\log 1]_T = 0$.

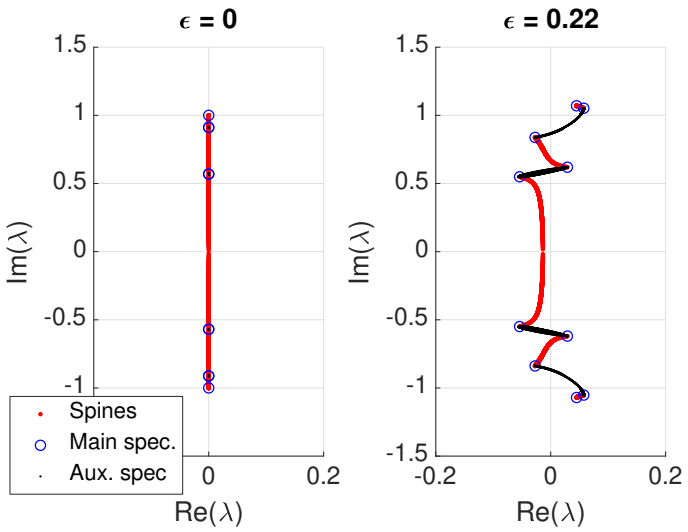

FIGURE 1. NONLINEAR SPECTRUM OF THE PLANE WAVE (25) WITHOUT AND WITH PERTURBATION.

After adding the perturbation, we obtain the nonlinear spectrum in Fig. 1(right). The four degenerate points have split up, leading to four new spines that that do not cross the real axis. The formerly trapped auxiliary spectra are freed and now contribute to the signal. We close this section with a few more properties of the nonlinear spectrum.

- The nonlinear spectrum is symmetric with respect to the real axis. Later only the region $\mathrm{Im}(\lambda) \geq 0$ is shown.
- There are more degenerate points in main spectrum on the real axis. However, these are not important here.
- Periodic solutions of the NSE are in general not finite gap, but can be approximated by finite gap solutions.
- Not all combinations of the parameters E_k and initial values $\mu_k(X_0,T_0)$, $\vartheta_k(X_0,T_0)$ lead to a periodic solution of the NSE. Conditions are provided in [24] .

NFT for the periodic NSE

The NFT for the NSE (19) with periodic boundary condition (20) takes one period of a finite gap solution,

$$u(X_0,T+T_0), \quad 0 \leq T < \ell, \quad X_0,T_0 \text{ fixed}, \tag{26}$$

and returns the constants E_k, initial values $\mu_k(X_0,T_0)$ for the auxiliary functions and the Riemann sheet indices $\vartheta_k(X_0,T_0)$. Given these values and $u(X_0,T_0)$, we can recover $u(X_1,T)$ for any desired value of X_1 in three steps:

1) Solve (23) for $\mu_k(X_1,T_0)$.
2) Solve (22) for $\mu_k(X_1,T)$, $T_0 \leq T < T_0+\ell$.
3) Use (24) to recover $u(X_1,T)$, $T_0 \leq T < T_0+\ell$.

Note that the Steps 2 and 3 together already constitute an *inverse NFT*. They can be implemented numerically. Also note that the spatial and temporal evolution are decoupled; we can restrict ourselves to a fixed $T = T_1$ in Step 1.

Inverse NFT using Theta Functions

Instead of solving (23) numerically and using (24) in order to implement an inverse NFT, it is also possible to solve (22)–(23) analytically using so-called *Theta functions*

$$\Theta(z \mid B) := \sum_{m_1,m_2,\ldots,m_g=-\infty}^{\infty} \exp\left(\pi \mathrm{i} z^T B z + 2\pi \mathrm{i} m^T z\right), \tag{27}$$

where the complex $g \times g$ matrix B is symmetric with negative definite imaginary part and m and z are column vectors with g entries. The m_i are the elements of the vector m and the superscript ^{T} denotes the transpose. It can be shown that for suitable choice of the matrix B and vectors a,b,c, (21) becomes $[\log u(X,T)]_T = \Theta(aX+bT+c \mid B)$ [25].

It is unfortunately quite difficult to obtain with this representation numerically. Since our software currently does not support it, we will not consider it further in this paper.

PHYSICAL INTERPRETATION OF THE NONLINEAR SPECTRUM

In the previous section, the NFT was introduced. Given a normalized time series $u(X_0,T)$, it returns a main spectrum consisting of constant complex points E_k, which are paired by constant curves known as spines, and initial conditions for a varying auxiliary spectrum $\mu_j(X,T)$. For the physical interpretation of the NFT, it is important to understand the relevance of *degenerate points* in the main spectrum.

Recall that a degenerate point in the main spectrum occurs when two connected points in the main spectrum coalesce. A degenerate point in the main spectrum may trap a point in the auxiliary spectrum that cannot move and thus does not contribute to the signal. However, any small perturbation can separate the two previously co-located points in the main spectrum so that the previously trapped point in the auxiliary spectrum is set free and can start to move. This behavior was illustrated in the previous section using the plane wave. An arbitrarily small perturbation can free auxiliary spectrum points trapped by degenerate points in the main spectrum and can thus lead to large changes as the wave evolves. Initial conditions that $u(X_0,T)$ that exhibit degenerate (non-real) points in the main spectrum can thus be susceptible to *modulational instability*. On the other

hand, if all (non-real) points in the main spectrum are non-degenerate, modulational instability does not occur. Classic works discussing these points in depth are e.g. [26, 19]. More recent references are, e.g., [27], [3, Ch. 24], [12].

Another important aspect is that, when considered in isolation, spines that do cross the real line correspond to stable modes in the sea state, while spines that do not cross the real line correspond to unstable modes [4, 28, 3, 13]. An extensive discussion of the interpretation of the spines is provided in the recent study [13].

The NFT has in particular been used to gain insight into the rogue wave phenomenon. Short spines that do not cross the real axis indicate that one is close to an unstable situation with degenerate main spectrum. Such spines have been found to be an important indicator for the presence of rogue waves even if these rogue waves were not visible at the location where the measurement was taken [5, 6, 7]. The classical breather solutions to the NSE, which are considered prototypes for rogue waves, are known to have highly degenerate main spectra [10, 9].

THE SOFTWARE LIBRARY FNFT

FNFT [14] is a software library for the numerical computation of NFTs. It in particular contains an algorithm for the computation of the NFT for the periodic NSE as discussed in the previous section that is based on [29]. Given a normalized time series with D samples

$$u_n := u(X_0, T_0 + n d_T), \quad n \in \{0, 1, \ldots, D-1\},\ d_T := \frac{\ell}{D}, \quad (28)$$

the routine `fnft_nsep` computes the corresponding main spectrum E_k and auxiliary spectrum $\mu_k(X_0, T_0)$. (The same routine has recently been used to analyze rogue waves in optical fiber in [30].) For this paper, a new option to visualize spines has been added. FNFT is mostly written in the programming language C, but interfaces to MATLAB and Python are available for convenience. More information on obtaining and installing FNFT is available online at `https://github.com/FastNFT/FNFT`. The figures shown in this paper were obtained using version 0.3.0 of FNFT.

In this paper, we demonstrate the use of FNFT via the MATLAB interface. The following script, which reproduces much of Fig. 1(right), demonstrates the basic usage.

```
%%% Setup
P = [0, 2*pi/0.822];     % period vec [T0,T0+l]
D = 256;                 % num. samples
dT = (P(2) - P(1)) / D; % step size
T = dT*(0:D-1);          % time grid
u = 1 + 0.22*exp(-0.822j*T); % signal
kappa = +1;              % focusing NSE

%%% Compute spines, main and aux. spectrum
spines = mex_fnft_nsep(u, P, kappa, ...
  'points_per_spine', 100);
[mainspec, auxspec] = mex_fnft_nsep(...
  u, P, kappa);

%%% Plot results
plot(real(spines), imag(spines), '.r', ...
  real(mainspec), imag(mainspec), 'ob', ...
  real(auxspec), imag(auxspec), '.k');
xlabel('Re(\lambda)'); ylabel('Im(\lambda)');
xlim([-0.2 0.2]); ylim([-1.5 1.5]);
```

The first part of the script computes the samples (28) of the signal (25). The second part calls FNFT to compute the spines, main and auxiliary spectrum of the signal. Finally, the results are plotted. (For more information about the interface to FNFT, run the command `help mex_fnft_nsep` in MATLAB.) One difference between Fig. 1(right) and the resulting plot is that does not show the complete loci of the auxiliary spectrum, $\mu_k(X_0, T)$ with $0 \le T \le \ell$, but only a few points $\mu_k(X_0, T_0)$. Full loci can be obtained by rerunning the process for different base points T_0 until $\mu_k(X_0, T_0)$ is known at all T_0 of interest, which is essentially a simplified (and less effective) version of a technique known as base point iteration (e.g. [3, Ch. 17.5.3]). We skip details since these loci will not of interest in the following. We remark that the result can be verified by comparing the plot [or Fig. 1(right)] with Fig. 4b in [10], where the same nonlinear spectrum has been computed with a different numerical method. A good agreement can be observed (note that the spectrum there is mirrored due to a slightly different definition of the NFT).

ANALYSIS OF FREE SURFACE BUOY DATA

In the following, we demonstrate how real-world data can be analyzed using FNFT. The data is collected by buoys operated by the Coastal Ocean Monitoring Center (COMC), National Cheng Kung University in Tainan, Taiwan. The chosen buoy was located in the northeast of Taiwan at a water depth of h=20 m. Every hour an recording of 10 minutes is taken with a sampling rate of 2 Hz. For this analysis, recordings for which deep water conditions hold ($k_0 h \gtrapprox 1.363$) were chosen. We consider the time series in Fig. 2, which was recorded on June 16, 2011, at 02:00.

We start our analysis with the following MATLAB code.

```
%%% Load dimensional data from text file (one
a = load('11071602.ELA'); %%% sample per row)
a = reshape(a, 1, []);  % convert to row vector
```

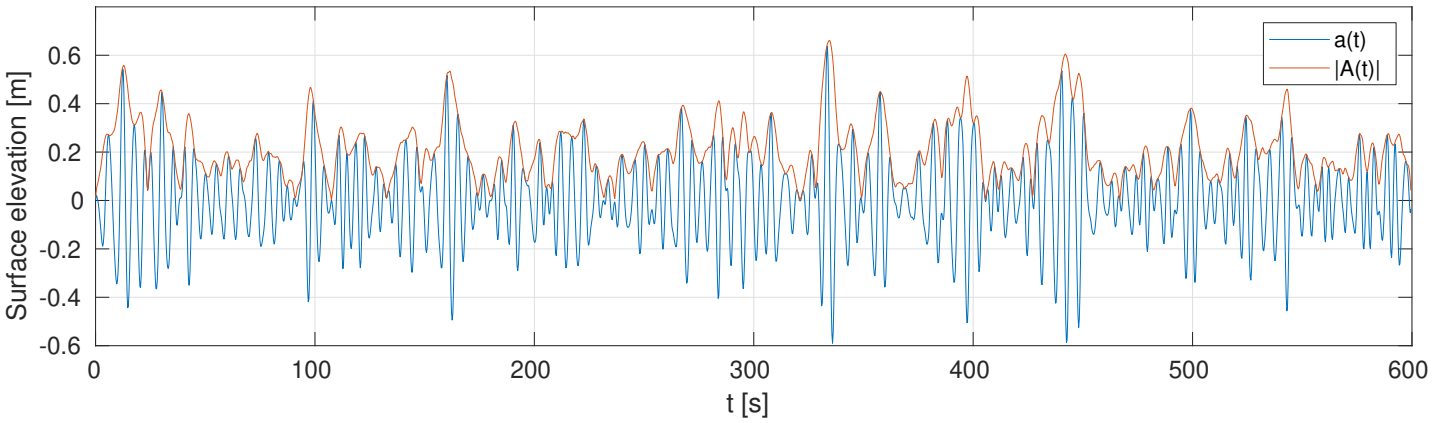

FIGURE 2. TIME SERIES USED FOR THE ANALYSIS AND MAGNITUDE OF THE CORRESPONDING COMPLEX ENVELOPE.

```
D = length(a);              % number of samples
assert(mod(D, 2)==0);       % D should be even

%%% Setup parameters
Fs = 2;                     % sampling frequency [Hz]
Ts = 1/Fs;                  % sampling period [s]
h = 20;                     % water depth [m]
g = 9.81;                   % gravitational acc. [m/s^2]
P = [0 (D+1)*Ts];           % begin and end of period
kappa = +1;                 % focusing NSE

% Oversample signal since mex_fnft_nsep needs it
% to be a power of two by zero-padding the FFT
Y = fft(a);
Dnew = 2^nextpow2(D);
Y = [Y(1:D/2) zeros(1,Dnew-D) ...
   Y(D/2+1:end)]*Dnew/D;
a_new = real(ifft(Y));
t_new = (0:Dnew-1)*Ts*(D-1)/(Dnew-1);

% Compute complex envelope (still with
% carrier) using the Hilbert transform.
A_with_carrier = hilbert(a_new);

% Compute sampling freq and freq grid for
% a_new (run "doc fft" for more info)
Fs_new = 1/(t_new(2) - t_new(1));
f_new = Fs_new*[(0:Dnew/2) (-Dnew/2+1:-1)]/Dnew;

% The peak of the spectrum provides the carrier
% frequency and wave number [Osborne 2010, 13.3]
[~,i] = max(abs(fft(A_with_carrier)));
w0 = 2*pi*f_new(i); k0 = w0^2/g;

% Remove the carrier to obtain A
A = exp(-1j*w0*t_new).*A_with_carrier;
```

The interpolation method used in the middle of this script is known as band-limited interpolation. The last part of the script implements (3) for $x = 0$. Note that the sign of ω_0 is switched as we are considering a time series (see the remark below (11)). The absolute value of the resulting complex envelope $A(t)$ is also shown in Fig. 2. We continue our analysis with the follwing MATLAB script.

```
% Compute parameters for the normalization
assert(k0*h>1.363); % check for deep water
s = tanh(k0*h); sx = 1-s^2; c = w0/k0;
Cg = c/2*(1+sx*k0*h/s); mu = -g/(8*k0*s*w0)* ...
     ((s-k0*h*sx)^2+4*k0^2*h^2*s^2*sx);
nu = -k0^4/2/w0*(c/2/s)^2*((9-10*s^2+9*s^4)/ ...
   2/s^2+(4*c^2+4*sx*c*Cg+g*h*sx^2)/(Cg^2-g*h));

% Normalize signal and compute spines, spectra
rho = Cg*sqrt(nu/2/mu); u = rho*reshape(A,1,[]);
spines = mex_fnft_nsep(u, P, kappa, ...
   'points_per_spine', 1000);
[main_spec, aux_spec] = mex_fnft_nsep(u, P, +1);
```

This script normalizes the complex envelope $A(t)$ using (6)–(8) and (12). Then, we compute the spines and the main spectrum as already described in the previous section. The resulting nonlinear spectrum is shown in Fig. 3.

Finally, we plot the conventional linear spectrum of the complex envelope for a comparison using the script below.

```
% Plot results with scaled axes for easier
% comparison with the nonlinear spectrum.
figure;
stem(-(2*pi*f_new)/2, abs(rho*fft(A)/Dnew));
xlabel('-\pif [Hz]'); xlim([-0.8 0.3]); grid on;
ylabel('\rho|A(f)|'); ylim([-1e-5 0.0045]);
```

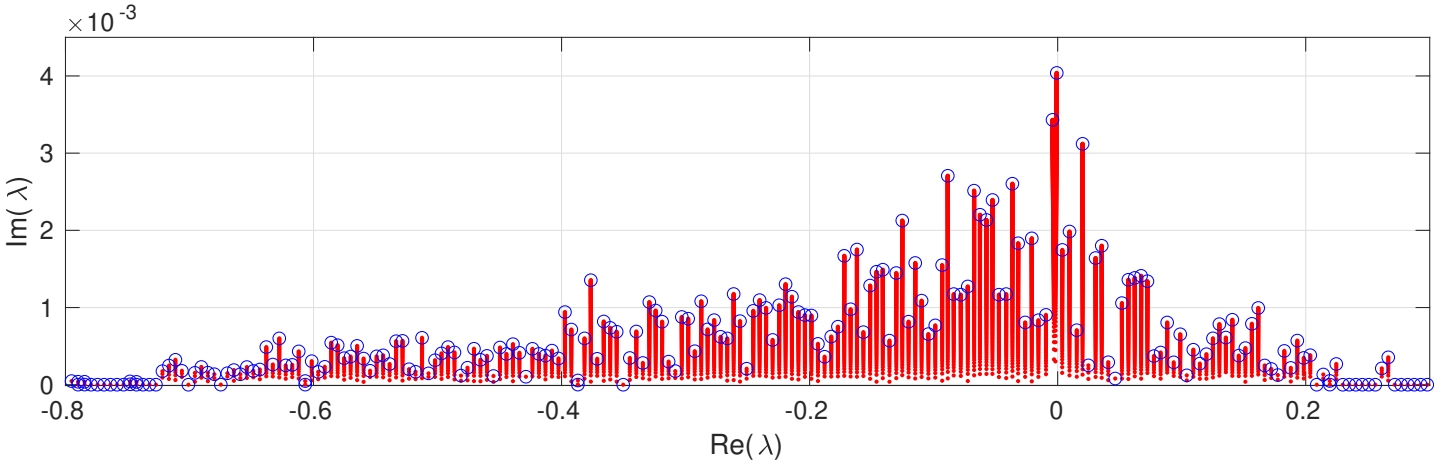

FIGURE 3. NONLINEAR SPECTRUM FOR THE COMPLEX ENVELOPE OF THE SURFACE ELEVATION SHOWN IN FIG. 2.

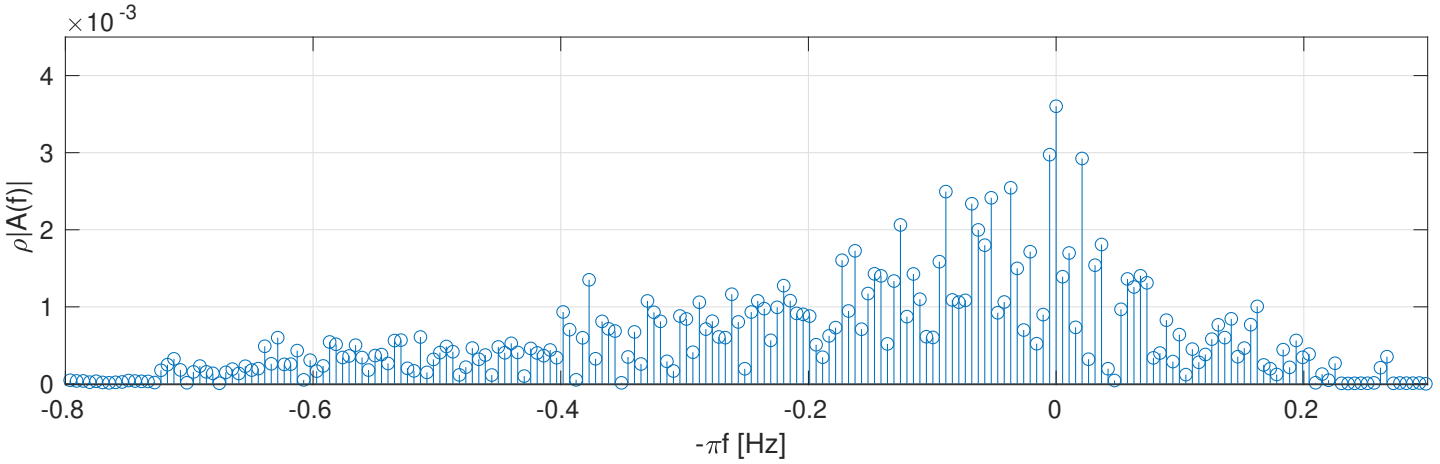

FIGURE 4. RESCALED LINEAR SPECTRUM FOR THE COMPLEX ENVELOPE OF THE SURFACE ELEVATION SHOWN IN FIG. 2.

The result is shown in Fig. 4. Since for very small wave envelopes it is known that the NFT reduces to a kind of Fourier series with $\mathrm{Re}(\lambda) \approx -2(2\pi f)$, we have scaled the horizontal axis accordingly for easier comparison with Fig. 2. Similarly, since we analyzed $u = \rho A$ nonlinearly, the vertical axis is scaled by ρ. Since we removed the carrier earlier, the zero frequency corresponds to the carrier frequency. In our case, it was $\frac{\omega_0}{2\pi} \approx 0.17$ Hz. We observe that the two spectra are very similar, which suggests that nonlinear effects are weak in this case. In particular, we cannot observe any unstable modes in the nonlinear spectrum (the spines all cross the real axis). For a more detailed analysis of another case with strong nonlinearity, we refer to [13].

CONCLUSION

In this paper, the background for using the NSE as a model for deep-water wave trains and the NFT for the periodic NSE as a tool to analyze corresponding data has been surveyed. We explicitly demonstrated how the software library FNFT can be used to perform such an analysis, and compared the results to a conventional linear analysis. We remark that FNFT is under constant development. In particular, we are working to improve support for KdV-NFTs.

ACKNOWLEDGMENT

This project has received funding from the European Research Council (ERC) under the European Union's Horizon 2020 Research and Innovation Programme (grant agreement No 716669).

REFERENCES

[1] Gardner, C. S., Greene, J. M., Kruskal, M. D., and Miura, R. M., 1967. "Method for solving the Korteweg-deVries equation". *Phys. Rev. Lett.,* ***19***(19), p. 1095.

[2] Zakharov, V., and Shabat, A., 1972. "Exact theory of two-dimensional self-focusing and one-dimensional self-modulation of waves in nonlinear media". *Soviet physics JETP,* ***34***(1), p. 62.

[3] Osborne, A., 2010. *Nonlinear Ocean Waves and the Inverse Scattering Transform*, Vol. 97. Academic Pr.

[4] Osborne, A. R., 2001. "The random and deterministic dynamics of 'rogue waves' in unidirectional, deep-water wave trains". *Mar. struct.,* ***14***(3), pp. 275–293.

[5] Islas, A. L., and Schober, C. M., 2005. "Predicting rogue waves in random oceanic sea states". *Physics of Fluids,* ***17***(3), p. 031701.

[6] Calini, A., and Schober, C. M., 2017. "Characterizing JONSWAP rogue waves and their statistics via inverse spectral data". *Wave Motion,* ***71***, pp. 5–17.

[7] Islas, A., and Schober, C. M., 2018. "Nonlinear spectral analysis of chaotic dynamics and rogue waves: Deep water wave and optics applications". *AIP Conference Proceedings,* ***2025***(1), p. 040010.

[8] Mohtat, A., Yim, S. C., Osborne, A. R., and Chen, M., 2018. "Nonlinear deepwater extreme wave height and modulation wave length relation". In ASME OMAE.

[9] Grinevich, P. G., and Santini, P. M., 2018. "The finite gap method and the analytic description of the exact rogue wave recurrence in the periodic NLS Cauchy problem. 1". *Nonlinearity,* ***31***(11), oct, pp. 5258–5308.

[10] Randoux, S., Suret, P., Chabchoub, A., Kibler, B., and El, G., 2018. "Nonlinear spectral analysis of Peregrine solitons observed in optics and in hydrodynamic experiments". *Phys. Rev. E,* ***98***, Aug, p. 022219.

[11] Brühl, M., and Becker, M., 2018. "Analysis of subaerial landslide data using nonlinear Fourier transform based on Korteweg-deVries equation (KdV-NLFT)". *Journal of Earthquake and Tsunami,* ***12***(02), p. 1840002.

[12] Grinevich, P. G., and Santini, P. M., 2019. "The finite-gap method and the periodic NLS Cauchy problem of anomalous waves for a finite number of unstable modes". *Russ. Math. Surv.,* ***74***(2), apr, pp. 211–263.

[13] Osborne, A. R., Resio, D. T., Costa, A., de León, S. P., and Chirivì, E., 2019. "Highly nonlinear wind waves in Currituck Sound: dense breather turbulence in random ocean waves". *Ocean Dyn.,* ***69***(2), pp. 187–219.

[14] Wahls, S., Chimmalgi, S., and Prins, P. J., 2018. "FNFT: A software library for computing nonlinear Fourier transforms.". *J. Open Source Software,* ***3***(23), p. 597.

[15] Whitham, G. B., 1974. *Linear and nonlinear waves*, Vol. 42. John Wiley & Sons.

[16] Melville, W. K., 1983. "Wave modulation and breakdown". *Journal of Fluid Mechanics,* ***128***, p. 489–506.

[17] Zakharov, V. E., 1968. "Stability of periodic waves of finite amplitude on the surface of a deep fluid". *J. Appl. Mech. Tech. Phys.,* ***9***(2), Mar, pp. 190–194.

[18] Hasimoto, H., and Ono, H., 1972. "Nonlinear modulation of gravity waves". *Journal of the Physical Society of Japan,* ***33***(3), pp. 805–811.

[19] Tracy, E., Larson, J., Osborne, A., and Bergamasco, L., 1988. "On the nonlinear Schrödinger limit of the Korteweg-de Vries equation". *Physica D: Nonlinear Phenomena,* ***32***(1), pp. 83–106.

[20] Yuen, H. C., and Lake, B. M., 1982. "Nonlinear dynamics of deep-water gravity waves". Vol. 22 of *Advances in Applied Mechanics*. Elsevier, pp. 67 – 229.

[21] Mei, C. C., 1983. *The Applied Dynamics of Ocean Surface Waves*. John Wiley & Sons.

[22] Matveev, V. B., 2008. "30 years of finite-gap integration theory". *Philos. Trans. R. Soc. London, Ser. A,* ***366***(1867), pp. 837–875.

[23] Kotlyarov, V., 1976. "Periodic problem for the Schrödinger nonlinear equation". *Voprosy Matematicheskoi Fiziki i Funkcionalnogo Analiza,* ***1***, pp. 121–31. English translation: arXiv:1401.4445.

[24] Tracy, E. R., Chen, H. H., and Lee, Y. C., 1984. "Study of quasiperiodic solutions of the nonlinear Schrödinger equation and the nonlinear modulational instability". *Phys. Rev. Lett.,* ***53***, Jul, pp. 218–221.

[25] Its, A., and Kotljarov, V., 1976. "Explicit formulas for solutions of Schrodinger nonlinear equation". *DOPOV AKAD NAUK A*(11), pp. 965–968. English translation: arXiv:1401.4445 (2nd half of the pdf).

[26] Forest, M. G., and Lee, J.-E., 1986. "Geometry and modulation theory for the periodic nonlinear Schrodinger equation". In *Oscillation Theory, Computation, and Methods of Compensated Compactness*. Springer, pp. 35–69.

[27] Bronski, J. C., and Rapti, Z., 2005. "Modulational instability for nonlinear Schrodinger equations with a periodic potential". *arXiv preprint nlin/0504052*.

[28] Ablowitz, M., Hammack, J., Henderson, D., and Schober, C., 2001. "Long-time dynamics of the modulational instability of deep water waves". *Physica D: Nonlinear Phenomena,* ***152***, pp. 416–433.

[29] Wahls, S., and Poor, H. V., 2015. "Fast numerical nonlinear fourier transforms". *IEEE Transactions on Information Theory,* ***61***(12), pp. 6957–6974.

[30] Goossens, J.-W., Hafermann, H., and Jaouën, Y., 2019. "Experimental realization of Fermi-Pasta-Ulam-Tsingou recurrence in a long-haul optical fiber transmission system". *Scientific Reports,* ***9***(1), pp. 1–11.